A Y-band Coherent Transceiver IC for OCS Spectroscopy Enabling Mixer-Based Odd-Order Dispersive Readout in CSMCs

*Shang-Xuan Chen[#$], Xu Cheng[#$], Liang Zhang[#$], Feng-Jun Chen[#$], Zhuo-Heng Chen[#$], Xian-Hu Luo[#$], Jiang-An Han[#$], Yun-Bo Rao[#$], Yi Jiang[#], Meng Jia[#$], Yun Fang[^£], Bo Wei[*], Binbin Cheng[#$], Xian-Jin Deng[#$], Hao Gao[^£2]

[#]Microsystems&Terahertz Research Center, CAEP, P.R.China

[$]Institute of Electronic Engineering, CAEP, P.R.China

[^]Purple Mountain Lab, P.R.China

[£]Southeast University, P.R.China

[*]Hangzhou Dianzi University, P.R.China

[&]Authors Shang-Xuan Chen and Xu Cheng contributed equally to this work

[1]chengxu_mtrc@caep.cn, [2]h.gao@seu.edu.cn

***Abstract*—This paper presents a Y-band coherent transceiver IC intended for high-order dispersion readout of the carbonyl sulfide (OCS) rotational transition in a chip-scale molecular clock (CSMC). A homodyne transceiver IC architecture is designed, incorporating a low noise amplifier (LNA), a down-conversion mixer, an 8× frequency multiplier, and a power amplifier, with a 90° coupler inserted for coherent detection while baseband signal processing is delegated to scientific instruments for radio frequency (RF) performance verification. Compared to previous reports on CSMCs, this prototype offers two distinct advantages: (1) coherent detection preserves amplitude, frequency, and phase information, which not only supports diverse modulation schemes but also facilitates high-order dispersion detection—an essential key to solving baseline drift. (2) the integration of an LNA improves the noise figure (NF) compared to square-law detectors, thereby enhancing the transceiver's signal-to-noise ratio (SNR), which is critical to the frequency stability of CSMCs. Implemented in a 130-nm SiGe BiCMOS technology, the transceiver IC delivers a maximum output power of 0.6 dBm @ 214 GHz and a minimum NF of 14.7 dB @ 218 GHz over a -3 dB bandwidth of 208~233.5 GHz, with a total power consumption of 185 mW in transmitter mode and 111 mW in receiver mode. To verify the practicality of this transceiver IC, a CSMC prototype was designed with an OCS gas cell and measured at an absorption line of ~218.9 GHz. The measured results demonstrate a start-up time of ~2 s, an Allan deviation of ~2.1×10^{-10} at 10 s, and ~5.2×10^{-11} at 1000 s, respectively. To the best of the authors' knowledge, this is the first demonstration of coherent OCS high-order dispersion interrogation.**

Keywords—chip-scale molecular clock (CSMC), coherent/heterodyne readout, odd-order dispersion, sub-THz transceiver.

I. Introduction

As depicted in Fig. 1, timekeeping standards have undergone continuous evolution from astronomical references, mechanical clocks, and quartz oscillators to quantum frequency standards represented by atomic clocks, motivated by the relentless pursuit of enhanced timing accuracy and superior frequency stability. The advancement of timekeeping technologies has facilitated the emergence of physical references with higher operating frequencies, higher quality factors (Q), and improved stability, which have enabled orders-of-magnitude suppression of daily time deviations [1]. In recent years, driven by the concurrent requirements for high precision, high stability, and miniaturized form factors, extensive research has been devoted to

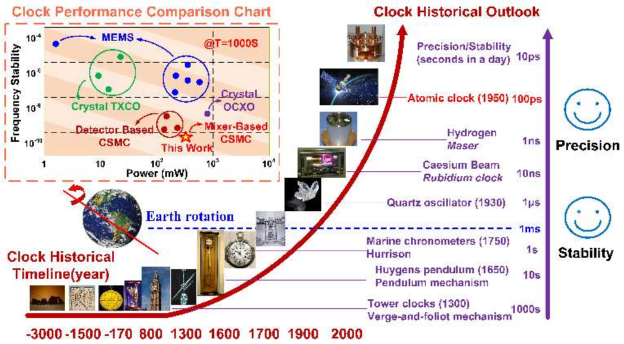

Fig. 1. Timeline of human timekeeping evolution and comparison chart between different Clocks.

chip-scale atomic clocks (CSACs) and chip-scale molecular clocks (CSMCs) [2]-[4]. Although CSMCs still exhibit deficiencies relative to CSACs in several critical performance indicators, their exceptional potential for miniaturization renders them promising portable candidates for timing applications in GPS-denied environments, while their optimal architectural design remains to be explored.

In previous CSMC readout demonstrations, square-law detectors have typically been employed for the sake of simplicity. Such detectors, however, are inherently vulnerable to baseline drift—arising from amplitude fluctuations, DC drift of single-ended crystal oscillators, and other associated factors—which imposes a significant constraint on the long-term stability of CSMC systems. Despite this critical limitation, only a handful of optimization attempts have been reported in the literature [4]-[7], with no systematic solutions proposed to address this issue. More importantly, square-law detection inherently discards frequency and phase information and exhibits intrinsic insensitivity to odd-order dispersive signatures, which can be effectively leveraged to mitigate baseline drift and enhance the long-term stability of CSMC systems [5]-[6].

To address these limitations and explore the optimal molecular detection scheme, this work adopts a Y-band coherent mixer-based readout transceiver topology, replacing the conventional square-law detector-based architecture. Specifically, the transmitter delivers an amplified, 8×-

multiplied modulated THz signal to probe the carbonyl sulfide (OCS) absorption line, while the receiver enables phase-sensitive extraction of odd-order dispersive modulation components. This design integrates an LNA to improve noise figure (NF) and signal-to-noise ratio (SNR), thereby addressing the baseline drift issue highlighted earlier and enhancing CSMC frequency stability in Fig. 1. The efficacy of this proposed Y-band coherent topology is further validated through CSMC demonstration measurements.

II. Comparison of a Mixer-Based and a Square-Law-Detector-Based Transceiver

A conventional square-law detector-based CSMC architecture and the proposed mixer-based counterpart are illustrated in Fig. 2. In both architectures, a voltage-controlled crystal oscillator (VCXO) combined with a phase-locked loop (PLL) generates a modulated signal at ~28 GHz. This signal is subsequently upconverted and amplified to yield a probing signal centered at ~218.9 GHz, which is employed to interrogate the OCS absorption line within the OCS gas cell. After propagating through the OCS gas cell, the filtered probing signal is routed to either a square-law detector or a mixer-based coherent receiver for down-conversion and baseband signal extraction. Finally, the recovered baseband signal is processed by an off-chip mixed-signal loop to calibrate the VCXO in a real time manner.

Qualitatively, the fundamental distinction between the two architectures lies in their readout mechanisms. In the proposed mixer-based transceiver, a 90° coupler introduces a precisely controlled phase offset between the two signal paths, thereby enabling coherent detection and the extraction of odd-order dispersive error components at the mixer output. In contrast, the square-law-detector-based architecture performs amplitude-only detection, thereby discarding the phase information inherent carried by the molecular response. This core difference directly governs the performance metrics of the CSMC. In order to evaluate the performance of the CSMC, the frequency stability (characterized by the Allan deviation, σ_y) of passive clocks in the short-to-medium term ($\tau < 10^3$ s, where τ denotes the averaging time) adheres to the relationship 错误!未找到引用源。:

$$\sigma_y \propto \frac{1}{SNR \cdot Q \cdot \sqrt{\tau}} \tag{1}$$

where Q represents the quality factor of the molecular gas cell, SNR denotes the overall signal-to-noise ratio of the readout chain, and τ is the averaging time. Since the molecular Q is inherently determined by the OCS rotational transition and gas cell design, improving the clock stability at the transceiver level primarily depends on enhancing the effective readout SNR. In conventional square-law-detector-based CSMCs, SNR enhancement is fundamentally constrained by two key factors: (1) baseline drift-induced by amplitude fluctuations and slow gain variations-distorts the extracted error signal, thereby degrading long-term locking robustness; (2) inferior noise performance of the square-law detector limits the optimal noise figure (NF) of the receiver. To address these limitations, the proposed mixer-based coherent architecture not only enables high-order dispersive readout for baseline drift suppression but also achieves a lower receiver NF compared to its square-law-detector-based counterpart, thereby effectively enhancing the readout SNR and enhancing the frequency stability of the CSMC.

A. Architectural Realization of High-Harmonic-Order Interrogation of OCS Rotational Transition

In order to investigate the OCS absorption and dispersion characteristics around the carrier frequency ω_0, $A(\omega)$, $\phi(\omega)$ and $\Delta\omega(t)$ are adopted to depict the amplitude, phase and modulation information respectively. Thus, the sub-THz signal at the output of the OCS gas cell can be modelled as a complex line response:

$$x_{cav}(t) = \Re\{X_0 A(\omega_0 + \Delta\omega(t))\} e^{j[\omega_0 t + \int_0^t \Delta\omega(\tau) d\tau]} \tag{3}$$

where the X_0 is a physical constant. Afterwards, this signal x_{cav} enters square-law detector-based receiver or mixer based one in Fig. 2. In the upper half, the square-law detector's output is:

$$Z_{det}(t) = G(t) A^2(\omega_0 + \Delta\omega(t)) + B_A(t) \tag{4}$$

where $G(t)$ models multiplicative gain drift and B_A accounts for additive baseline drift. Therefore, the dispersive phase information Φ(ω) and the accompanying odd-order dispersive error signals cannot be directly accessed.

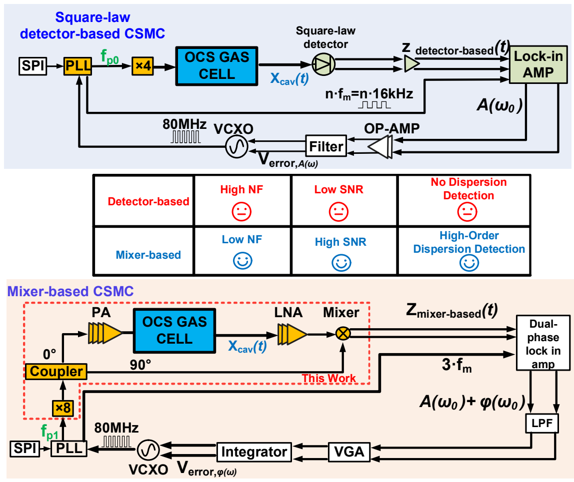

Fig. 2. An architectural comparison of a square-law detector-based CSMC (upper half) and a mixer-based one (lower half).

Meanwhile, in the lower half, the mixer's output is:

$$Z_{mixer}(t) = G_1 A(\omega_0 + \Delta\omega(t)) e^{j[(\omega_0 - \omega_{LO})t + \int_0^t \Delta\omega_m(\tau) d\tau]} \tag{5}$$

Where G_1 is the receiver front-end's conversion gain. Thus, both the amplitude information A(ω) and the phase information Φ(ω) is preserved. After performing quadrature synchronous demodulation via dual-phase lock-in amplifier at $3f_m = 3\frac{\omega_m}{2\pi}$, a high-order dispersive error signal is obtained:

$$V_{error,\phi(\omega)} \propto \frac{d^3\phi(\omega)}{d\omega^3} \tag{6}$$

Equation (6) shows that amplitude perturbations do not propagate to the phase error after $3\omega_m$ demodulation. According to (2) ~ (6), the output error signals of mixer-based ($V_{error,\ A(\omega)}$ in Fig. 2 upper half) and detector-based transceivers ($V_{error,\ \Phi(\omega)}$ in Fig. 2 lower half) are simulated in Fig. 3(a) and thus, mixer-based one enables error signal detection with a higher derivative slope compared to the other two without any baseline drift. In summary, a mixer-based coherent receiver not only extracts odd-order dispersive error components, but also effectively suppresses baseline drift and amplitude-modulation-induced perturbations, yielding a more stable readout signal and facilitating robust closed-loop locking in CSMC operation.

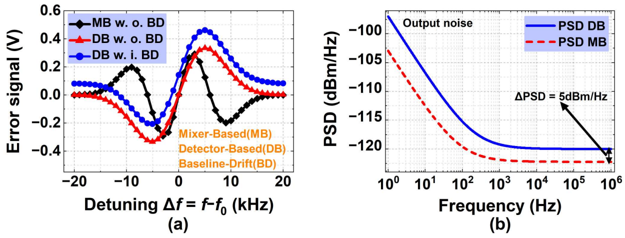

Fig. 3. A simulation comparison of mixer-based CSMC and detector-based one: (a) output error signal curves with and without baseline drift. (b) output power spectrum density of the two architectures.

B. Low noise of the Coherent Transceiver

The input-referred noise-equivalent power of the mixer-based receiver is:

$$P_{n.mixer-base} = k \cdot T_0 \cdot F_{mixer-base} \cdot B_{IF} \quad (7)$$

Where k is Boltzmann's constant, T_0 is $290K$, and $F_{mixer\text{-}based}$ is the noise factor of the receiver front-end referred to the RF input. B_{IF} denotes the effective noise bandwidth of the synchronous demodulation.

Meanwhile, the input-referred noise-equivalent power of detector-based receiver is:

$$P_{n.detector-based} = NEP^2 \cdot B_v \quad (8)$$

Where NEP is the detector noise-equivalent power ($W/\sqrt{Hz}$), B_v is the effective noise bandwidth of the detector baseband filter. (7) and (8) are simulated in Fig.3 (b) where an approximately ~5 dB difference in input-referred noise power spectrum density (PSD) at 1 MHz offset frequency is shown. In short, A coherent mixer-based receiver exhibits superior noise performance compared than that of a detector-based counterpart and thus, NF and SNR is simultaneously improved.

III. CSMC Architecture And Implementation

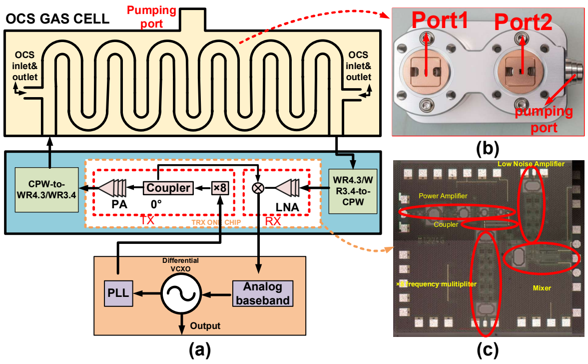

Fig. 4. Proposed CSMC: (a) CSMC architecture; (b) OCS gas cell; (c) transceiver IC photograph.

The proposed CSMC architecture is illustrated in Fig. 4(a) with its OCS gas cell in Fig. 4(b) and Y-band transceiver prototype IC in Fig. 4(c). In Fig. 4(a), a pumping port is used for vacuuming and gas filling on the top of the gas cell, while the left- and right-side ports serve as the OCS inlet and outlet respectively. In the middle part, the transceiver IC is wire bonded to the inlet and outlet of the OCS gas cell through two CPW-to-WR4.3 waveguide transitions. In the lower part, the low-frequency signal-generation and processing modules, including the PLL, differential VCXO, and analog baseband, are used to generate modulation signals and VCXO real-time calibration.

A. OCS Gas Cell Design

In order to enssure vaccum isolation and wideband coupling, a sapphire box-type window is adopted and sealed in the OCS gas cell. Without OCS filling and vacuum sealed, its S11 is lower than -15 dB with an S21 better than -5 dB over 210~260 GHz, thereby supporting low-reflection excitation and low-loss transmission. With OCS filled at a pressure of 40 Pa, the absorption line at 209.72/218.91/231.06 GHz is given in Fig. 5(b) while the optimum symmetrical one with lowest full width at half maximum (FWHB) is located ~218.9 GHz, where the error curve achieves its maximum slope and the peak absorption intensity is 25%.

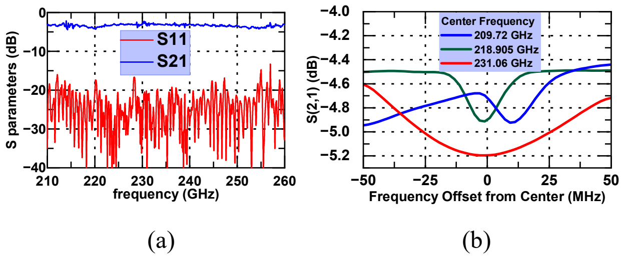

Fig. 5. OCS gas cell measurement. (a) S11 and S21 of the vacuum gas cell. (b) OCS absorption line at 209.72 GHz/218.91 GHz/ 231.06 GHz.

B. Transceiver IC Design

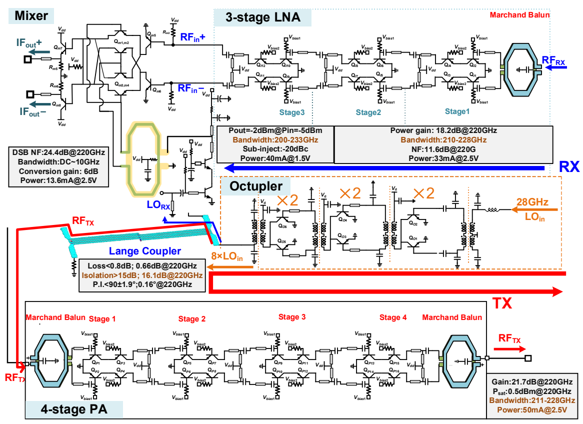

Fig. 6. Proposed transceiver IC architecture.

Fig. 6 shows a multiplier-based transceiver enabling odd-order dispersive readout with improved baseline robustness. A 28-GHz modulated signal is upconverted by an on-chip 8×

multiplier and split by a broadband 90° Lange coupler to drive the TX path and provide a phase-coherent LO for homodyne RX.

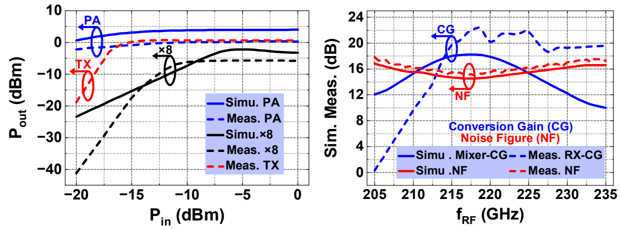

(a) (b)

Fig. 7. Y-band transceiver IC simulation and measurement results: (a) TX output power. (b) RX NF and conversion gain.

The receiver consists of a 3-stage differential LNA followed by a Gilbert-cell mixer, achieving 22.3-dB measured conversion gain and a minimum NF of 14.7 dB at 218 GHz. Meanwhile, the transmitter adopts a 4-stage differential PA and delivers 0.6-dBm saturated output at ~218 GHz, sufficient for molecular excitation while avoiding power-induced line broadening. Thus, the stability improvement mainly arises from RX NF reduction rather than increased TX power. The 8× multiplier covers 200-240 GHz with >20-dBc harmonic suppression.

IV. Measurement Results

Fig. 8 shows the CSMC prototype, where the mixer output is synchronously demodulated by dual-phase I/Q lock-in detection at $3f_m$, which shifts the discriminator extraction away from DC and improves baseline robustness. Fig. 9(a) summarizes the CSMC measurement setup, where the divided clock output is measured by a frequency counter referenced to a 10-MHz standard rubidium time base. Using the ~218.9-GHz absorption line, the prototype exhibits a startup time of ~2 s and achieves Allan deviations of 2.1×10^{-10} at 10 s and 5.2×10^{-11} at 1000 s [Fig. 9(b)].

(a) (b)

Fig. 8. The CSMC system: (a) top view without OCS gas cell. (b) top view with OCS gas cell.

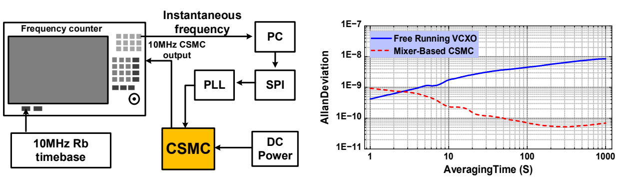

(a) (b)

Fig. 9. (a) Measurement setup. (b) Allan deviation.

V. Conclusion

This work presents a Y-band coherent transceiver IC for OCS spectroscopy in CSMCs. By preserving both the amplitude and phase information, the quadrature homodyne architecture enables $3f_m$ odd-order dispersive demodulation with improved baseline robustness over square-law detection. In addition, the mixer-based receiver with LNA improves sensitivity under saturation-limited probing power. The closed-loop prototype achieves Allan deviations of 2.1×10^{-10} at 10 s and 5.2×10^{-11} at 1000 s, which is among the best specifications in previous reports.

TABLE I. Comparison With Other CSMCs

Parameters	[7]	[6]	[5]	[4]	This Work
Architecture	Mixer-Based	Square-Law	Square-Law	Square-Law	Mixer-Based
ADEV [10^{-10}] τ = 10s	N/A	2.4	5.4	8.6	2.1
Freq. band [GHz]	220-233	220-240	220-240	211-229	208-228
TX. Psat [dBm]	-9	-10	-9.4	-20	0.6
RX. CG [dB]	14	N/A	N/A	N/A	22.3
RX. NF SSB [dB]	24	43.5	43	47	14.7dB
Area [mm²]	3.6	5	4.8	2.4	1.8
Power [mW]	175	71	70	66	95mA@2.5V 40mA@1.5V
Technology	65nm CMOS	65nm CMOS	65nm CMOS	65nm CMOS	130nm SiGe

Acknowledgment

The authors thank the support of National Natural Science Foundation of China (NSFC) under Grant U2430210, Key Research Program of Jiangsu Province under Grant BG2024035 and Mobile Information Networks National Science and Technology Major Project under Grant 2025ZD1305100.

References

[1] W. J. Riley, “Handbook of frequency stability analysis,” Nat. Inst. Standards Technol., Gaithersburg, MD, USA, NIST Special Publication 1065, 2008.

[2] D. Ruffieux et al., “A low-power fully integrated rf locked loop for miniature atomic clock,” in IEEE *ISSCC*, 2011.

[3] Zhang, H., et al. (2019). "ULPAC: A Miniaturized Ultralow-Power Atomic Clock." IEEE Journal of Solid-State Circuits 54(11): 3135-3148.

[4] C. Wang et al., “Chip-Scale Molecular Clock,” IEEE *JSSC*, 2019.

[5] C. Wang et al., “A terahertz molecular clock on cmos using high-harmonic-order interrogation of rotational transition for medium-/long-term stability enhancement,” IEEE *JSSC*, 2021.

[6] C. Wang et al “A sub- THz CMOS molecular clock with 20 ppt stability at 10,000 s based on dualloop spectroscopic detection and digital frequency error integration,” in Proc. IEEE Radio Freq. Integr. Circuits Symp. (RFIC)

[7] C. Wang et al., "CMOS Saturation Spectrometer With a Miniaturized Fabry–Pérot Cavity for the Lamb-Dip Interrogation of OCS Molecules to Enhance the Q of CSMC," in *IEEE Transactions on Microwave Theory and Techniques*